Copyright

by

Lekhaj Patha

2023

The Thesis Committee for Lekhaj Patha
Certifies that this is the approved version of the following Thesis:

Analyzing Voltage Sag Direction using Protective Relays and Deep-learning Methods

APPROVED BY
SUPERVISING COMMITTEE:

Surya Santoso, Supervisor

Brian Johnson

Analyzing Voltage Sag Direction using Protective Relays and Deep-learning Methods

by

Lekhaj Patha

Thesis

Presented to the Faculty of the Graduate School of

The University of Texas at Austin

in Partial Fulfillment

of the Requirements

for the Degree of

Master of Science in Engineering

The University of Texas at Austin

May 2023

Dedication

I dedicate this to my family, who have been a constant support throughout my life. Thank you for all your support along the way.

Acknowledgments

I would like to express my sincere gratitude to my academic advisor, Dr. Surya Santoso for his continuous support, motivation, and immense knowledge. The guidance helped me in all the time research and writing of the thesis. I would also like to thank Dr. Brian Johnson for reviewing my thesis and offering insightful comments on my research.

I would like to thank my colleagues in Dr. Santoso's research group. Thanks to Debjyoti Chatterjee, Woosung Kim, Moises Chong, and Eliot Ortega for the technical discussions and for providing constructive feedback on my research work. I would also like to thank my friend Aditya Raj for his support and motivation to learn deep learning.

Finally, I would like to thank my parents and my elder brother, whose unconditional love and guidance have supported me to be in this stage. Special thanks and love to my friends in India and Austin for their motivation and support for the completion of the thesis.

Abstract

Analyzing Voltage Sag Direction using Protective Relays and Deep-learning Methods

Lekhaj Patha, M.S.E

The University of Texas at Austin, 2023

Supervisor: Surya Santoso

As the electricity demand continues to grow, power systems are becoming more complex and interconnected, making the need for reliable protection systems more important than ever. Protection systems are designed to detect and isolate faults and other abnormal conditions, preventing them from cascading through the power grid and causing widespread outages. The primary challenge in protection is to detect the fault, the type of fault, and the location of the fault. Traditional relays effectively locate, detect, and isolate faults. Circuit breakers, fuses, and relays, these devices work together to ensure the power system remains stable and reliable, under various conditions including system failures. Smart Intelligent relays (SIRs) are designed to perform a broader range of functions, such as fault location, and power quality monitoring. Machine learning techniques are increasingly applied in power systems protection to enhance fault detection and classification accuracy and speed. ML algorithms can be used to analyze real-time data from sensors and other devices to detect and classify faults, including those that may be too small or subtle to be detected by traditional protection systems.

The thesis aims to study methods of identifying the direction of voltage sags in the distribution circuits. Voltage sags arise from the presence of short-circuit faults involving single, double, and three phase-to-ground conditions. The direction of the fault is based on the direction of power flow before the occurrence of the event. A fault can be classified as a downstream fault from a monitoring location if the direction of power flow is towards the fault location before the occurrence of the event. Similarly, a fault can be classified as an upstream fault if the direction of power flow is against the fault location before the occurrence of the fault. The terms upstream and downstream are relative to the monitor location. A downstream fault for one monitor can be an upstream fault for a different monitor. This thesis studies the applications of protective relaying and deep learning techniques in identifying the direction of voltage sags using the real-time waveforms of voltage and current to estimate whether the fault is upstream or downstream from the monitored location(s). The fault data was generated using a time-domain power system modeling tool with variable fault impedances and multiple fault locations. Relay-based approaches have been studied, and a deep-learning technique has been developed with the data generated. The relay-based techniques were capable of identifying the fault direction in all the cases irrespective of the fault location and fault duration. ML algorithms can help analyze large amounts of data and detect patterns that may be difficult or impossible for traditional protection systems to identify.

Table of Contents

List of Tables

List of Figures

Chapter 1: Introduction

Power system protection is a critical aspect of modern power systems, aimed at ensuring the safe and reliable operation of the power grid. It involves the use of various devices and technologies, such as relays, circuit breakers, fuses, and sensors, to detect and isolate faults, abnormal conditions, and other disturbances in power systems. Power system protection aims to prevent equipment damage, minimize outages, and maintain the quality of power delivered to customers. The protective relay market is estimated to be worth 14.7 billion by 2030, with a compound annual growth rate of 6.3% [1]. The continuous rise in energy consumption is being compensated with a continuous rise in electric power generation either by adding new conventional energy sources (coal, fuel, etc....) or by adding new renewable energy sources (Solar, wind, etc....). Similarly, the protection system must be improvised accordingly with an increase in demand.

1.1 BACKGROUND

Power system protection has become increasingly important due to the continuous increase in electricity demand, which has resulted in more complex and interconnected power systems. The protection system is designed to act quickly and decisively when an abnormal condition is detected, isolating the affected equipment, and preventing the spread of fault to other parts of the power system. This helps to minimize the impact of the faults and disturbances on the power grid and prevent cascading failures that can lead to widespread outages.

In electrical power systems, faults can cause unbalanced currents and voltages in the system, which can be difficult to analyze using traditional techniques. The three-

phase quantities in the power system (voltage and current) can be decoupled into sequence components (zero, positive, and negative). These sequence components are applied widely in power systems to estimate the stability of the system during an event. The event can be load disturbance, faults, overloading, and other outages. The positive sequence component represents the balanced component of the quantity that flows in phase with normal operating conditions of the system. The negative sequence component represents the balanced component of the quantity that flows in the opposite phase to the normal operating conditions of the system. The zero-sequence component represents the unbalanced component of the quantity that flows in a common mode through all phases of the system.

Several types of faults can occur in modern power systems, including the following types:

a) Open circuit faults
b) Short Circuit faults

The main reason behind the open conductor faults is a broken conductor and malfunctioning of the circuit breakers. The open circuit faults can further be classified into the following types:

a) Open conductor fault
b) Two conductors open fault
c) Three conductors open fault

The short-circuit fault occurs when a low-resistance path is created between two or more conductors in a power system. This results in a large current flow, which can

damage equipment and cause power outages. Short circuit faults can be further classified into the following types:

Sl. No	Type of faults	Notation	Symmetry	Probability of occurrence
1.	Line to ground	LG	Unsymmetrical	70-80%
2.	Line to line	LL	Unsymmetrical	15-20%
3.	Double Line to ground	LLG	Unsymmetrical	<10%
4.	Three-phase line to line	LLL	Symmetrical	<1%
5.	The three-phase line to ground fault	LLLG	Symmetrical	2-3%

Table 1.1: Types of short-circuit faults in power system.

Table 1.1 [2] shows the type of short-circuit faults and their probability of occurrence in the power system. It can be observed that the line-to-ground (LG) faults are one of the most dominant faults in the system. In many cases, these faults are temporary faults that cause momentary voltage sags in the system. These temporary faults are handled by reclosers in the majority. The major effects of the faults in the power system are overcurrent flow, danger to the operators, loss of electrical equipment, electric fires, etc. The percentage of fault occurrence based on the elements of the power system is classified into the following types [3]:

Sl. No	Element	Probability of occurrence
1.	Transformers	10
2.	Overhead lines	50
3.	Underground cables	9
4.	Switchgear	12
5.	CT, PT relays, Control equipment, etc.	12
6.	Generators	7

Table 1.2: Probability of occurrence of power system faults based on the elements.

1.2 MOTIVATION

The main objectives of power system protection are to ensure the power systems' safety, reliability, and efficiency. With advances in technology, such as digital relays and intelligent protection systems, power system protection has become more accurate and faster in detecting and responding to faults and disturbances.

Machine learning (ML) has become a popular tool in many applications due to its ability to handle large amounts of data and identify patterns that may be difficult for humans to detect. In power system protection, ML techniques have been proposed to improve fault detection and response accuracy and speed. However, there are several reasons why ML may not be appropriate for power system protection. Power systems are highly complex and nonlinear, making developing accurate and reliable ML models

difficult. Moreover, the lack of transparency in ML models can make understanding the reasoning behind protection decisions difficult. This is a critical issue in power system protection, where decisions must prioritize safety and reliability. ML models can be prone to errors and biases, which could lead to incorrect or unsafe decisions. Developing a robust and reliable ML model for power systems could be challenging, especially given the heavy regulation of power systems and the need for regulatory approval.

While ML has potential in many areas, there are significant challenges to its use in power system protection. Further research and development will be needed to overcome these challenges and ensure that any ML models used for power system protection are safe, reliable, and effective. In the meantime, traditional protection methods, such as relay-based protection, will continue to play a crucial role in ensuring power systems' safe and reliable operation.

Chapter 2: Literature Review

The electric power system can briefly be divided into three sub-systems: generation, transmission, and distribution. The electric power is generated in a power generation plant and transmitted using the transmission system which is then distributed using the distribution systems. A short-circuit fault may occur in any of the three sub-systems and it is unavoidable due to natural scenarios. The fault causes the electric power to pass through a different path, which further causes damage to the equipment and power interruption. The continuous power supply can be maintained by identifying and isolating the faulty region. There are numerous techniques available to identify the location of the fault as follows:

- Traveling wave methods [4]
- Impedance methods [5]
- Synchronize voltage and current measurements [6]
- Sparse measurement methods [7]
- Artificial Neural Network (ANN) methods [8]
- Support Vector Machines (SVMs) [9]
- Genetic algorithms [10]
- Convolutional neural networks [11]
- Integrated methods [12]

The techniques mentioned above have multiple advantages and disadvantages [13]. Some methods are very practical and deployable in real-world scenarios, and some might be more accurate for a particular system. The above-mentioned methods use

various data depending on their operation in the phase domain or sequence domain. In this literature review, impedance methods are studied extensively to evaluate the accuracy in identifying the relative fault location of a short-circuit fault.

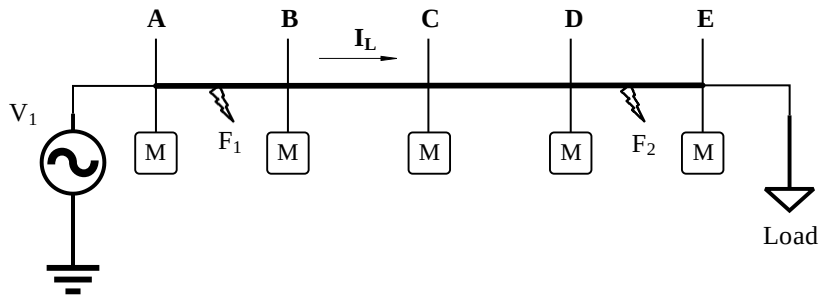

Figure 2.1: Single-line diagram of a five-node bus system

Fig. 1.1 shows a single-line diagram of a five-node system with a voltage source V_1. The power flow is from the voltage source to the load as indicated by the direction of the current flow. The system consists of five power-quality monitors that monitor the three-phase voltages and currents. There are two faults F_1 and F_2 in the system. A fault can be classified as a downstream fault from a monitoring location if the power flow is towards the fault location before the occurrence of the fault. A downstream fault is also known as a forward fault. Similarly, an upstream fault can be classified from a monitoring location if the power flow is against the fault location before the occurrence of the fault. An upstream fault is also known as a reverse fault. The notation upstream and downstream is defined in Table 2.1 for the five-node system in Fig. 1.1.

Sl. No	Monitor Location	Fault location	
		F_1	F_2
1.	A	Downstream	Downstream
2.	B	Upstream	Downstream
3.	C	Upstream	Downstream
4.	D	Upstream	Downstream
5.	E	Upstream	Upstream

Table 2.1: Fault classification based on monitor location for five node system.

The five-node system has been implemented in the EMTP software. The upstream data has been generated using fault F_1. Fault F_1 is an A-phase to C-phase type fault with an impedance of 1 ohm and fault F_2 does not exist in the system for the generation of upstream fault data. Similarly, fault F_2 is an A-phase to C-phase type fault with an impedance of 1 ohm, and fault F_1 does not exist in the system for the generation of downstream fault data. The three-phase voltages and currents are measured at the power quality monitor at node C. These values are converted into the sequence components using (2.1). The variables in (2.1) are the r.ms. values and α is $1\angle 120°$.

$$\begin{bmatrix} V_0 \\ V_1 \\ V_2 \end{bmatrix} = \begin{bmatrix} 1 & 1 & 1 \\ 1 & \alpha & \alpha^2 \\ 1 & \alpha^2 & \alpha \end{bmatrix} * \begin{bmatrix} V_a \\ V_b \\ V_c \end{bmatrix} \tag{2.1}$$

Table 2.2 provides values of the negative sequence quantities which can be calculated using (2.1) at node C for the upstream and downstream faults. The values are as follows:

Sl. No	Measured quantity	Value	
		Upstream	Downstream
1.	V_2	2770.62 V	2189.26 V
2.	$\angle V_2$	132.29°	132.38°
3.	I_2	31.64 A	44.45 A
4.	$\angle I_2$	87.52°	-114.33°

Table 2.2: Negative sequence values for an upstream and downstream fault in the five-node system

2.1 NEGATIVE SEQUENCE TORQUE

The traditional electromechanical relays are improved into microprocessor-based relays [14]. These relays are deployed to identify the fault based on the torque produced by the relay. The torque measured by the relay is comparable to the torque measured by the electromechanical relays, but the quantities used are the negative sequence components of voltage and current. The unit of T32Q measured in (2.2) is VA but it is known as torque because of the similarities with the electromagnetic relays. The sequence components of the voltage and current can be obtained using (2.1). These relays use the transmission line's characteristic angle, also known as the maximum torque angle setting [14]. The maximum torque angle is the angle at which the torque produced by the relay is maximum. The torque can be calculated using the below equation:

$$T32Q = |V_2|\,|I_2| \cos\left(\angle - V_2 - (\angle I_2 + \angle MTA)\right) \qquad (2.2)$$

where:

T32Q = Torque produced

V_2 = Negative sequence voltage

I_2 = Negative sequence current

MTA = Characteristic angle of transmission line / maximum torque angle setting

A negative torque value indicates a reverse fault, also known as an upstream fault. Similarly, a positive value of the torque indicates a forward fault which is also known as a downstream fault. The terms forward/backward and upstream/downstream are defined based on the direction of power flow in the system. An upstream fault can also be a downstream fault if the location of the power quality monitor is changed, or the power flow direction is altered. The torque can be calculated using (2.2) and for the five-node system, the value of torque for the upstream fault is -66.92 kVA and the value of torque for a downstream fault is 92.4 kVA.

The main disadvantage of the above-mentioned directional relay is the usage of negative sequence voltage and current. A strong power source can be defined as an electric source with a lower source impedance, while a weak power source can be defined as an electric source with a high source impedance [14]. These definitions are determined based on the short circuit ratio of the generator. A strong source produces less magnitude of negative sequence voltages. When a fault occurs near the strong source, the magnitude of the negative sequence voltage produced is low. Thus, this is a significant drawback while implementing the above-mentioned negative sequence torque relays.

In this fault identification method, one of the major advantages is the polarity difference (positive or negative) in the torque calculated for upstream and downstream faults. Moreover, the other advantage is the high magnitude of difference in torque between upstream and downstream faults. One of the disadvantages of this type of fault identification method is implementing them during the three-phase faults. In a three-

phase fault, the negative sequence voltage produced is very low because the fault is a balanced fault. In a balanced fault condition, the magnitude of the negative sequence voltage is dependent on the individual loads on the three phases. If the unbalance in the load between the three phases is high, this method can be implemented easily, but in the power system, almost all the loads on the three phases are approximately balanced. Thus, this method is not an efficient method to detect whether the balanced fault is upstream or downstream. But this method is an efficient method to detect whether the unbalanced fault in the system is an upstream fault or downstream fault.

2.2 NEGATIVE SEQUENCE IMPEDANCE RATIO

As mentioned above, when the source behind the relay is strong (low impedance), the negative sequence voltage produced is low, which can cause the relay to malfunction. This phenomenon is observed in most of the remote faults. This drawback has been partially resolved by changing the threshold values in calculating the negative sequence impedance as mentioned below [15]:

$$Z_{2measured} = \frac{\mathrm{Re}\,[V_2 * (1\angle Z_1 * I_2)^*]}{|I_2|^2} \qquad (2.3)$$

where:

$Z_{2measured}$ = Impedance calculated

V_2 = Negative sequence voltage

I_2 = Negative sequence current

/_Z_1 = positive sequence line angle

In this approach, the ratio of negative sequence voltage and current has been used instead of the product of these quantities. The fault is declared when the measuring quantity is higher than the restrained quantity in an electromechanical relay. Similarly, the value of the impedance calculated can be compared to the $-Z_{S2}$ (source impedance behind the relay) and Z_{L2} (sum of line impedance and remote source impedance). The impedance Z_{S2} is the equivalent Thevenin negative sequence impedance of the source behind the relay. The impedance Z_{L2} is the equivalent Thevenin negative sequence impedance of the transmission line and source ahead of the relay. Based on the comparison, the fault be identified as an upstream fault or downstream fault. The positive value indicates an upstream fault, while a negative value indicates a downstream fault. The impedance $Z_{2measured}$ can be calculated using (2.3) and for the five-node system, the value of impedance for the upstream fault is 66.85 ohms and the value of torque for a downstream fault is -44.76 ohms.

Similar to the previous identification method, one of the major advantages is the polarity difference (positive and negative) for the impedance calculated for upstream and downstream faults. Similarly, one of the major disadvantages of this identification method is implementing the same for a three-phase fault. A three-phase fault is a balanced fault and the negative sequence voltage produced is based on the unbalance in the system as explained earlier. When the negative sequence voltage produced is low, the calculation of the impedance might give incorrect results. Thus, this method is not an efficient way to identify whether the balanced faults are upstream or downstream. But in case of an unbalanced fault, this method efficiently identifies whether the fault is upstream or downstream.

Chapter 3: Generation of short-circuit fault data and sensitivity analysis using the IEEE 34-Bus system

The IEEE 34-bus system was originally developed in 1992 and approved during the PES Summer meeting in the year 2000 [16]. This is an actual feeder located in Arizona, and the nominal voltages in the circuit are 24.9 kV and 4.16 kV. Fig. 3.1 circuit diagram represents the nodes in the IEEE 34-Bus system.

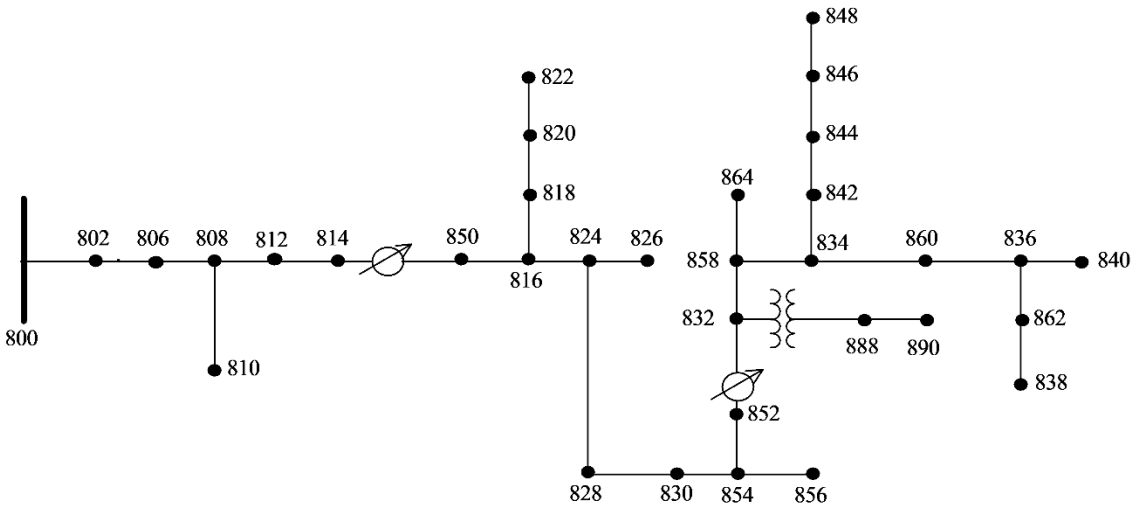

Figure 3.1: Single-line diagram of IEEE 34-Bus system.

3.1 GENERATION OF SIMULATED FAULT DATA FROM IEEE 34-BUS SYSTEM

The IEEE 34-Bus system mentioned above has been used to generate fault data in the software EMTP (Electromagnetic Transients Program). In the IEEE 34- Bus system, the wind power generator connected to node 848 and node 890 has been excluded. The original system is 24.9 kV, 12 MVA, 60 Hz with various types of fixed loads and distributed loads. The load type includes constant power, constant impedance, and constant current loads of both three-phase and single-phase). Moreover, the fault in the

system at node 890 has also been excluded for simplification of the model. The dynamic loads connected to node 888 have also been excluded from the system. The system has been initially solved using the power flow solution using the source connected to node 800 as the slack bus.

The fault data has been generated based on the power quality monitors located at nodes 800, 814, and 888. The raw voltage and current waveforms have been generated at the above-mentioned nodes for the faults at nodes 808, 824, 832, and 890. Based on the definition of upstream, downstream, and the monitor location and the fault location, the faults can be categorized as follows:

Sl. No	Monitor location	Fault location			
		808	824	832	890
1.	800	Downstream	Downstream	Downstream	Downstream
2.	814	Upstream	Downstream	Downstream	Downstream
3.	888	Upstream	Upstream	Upstream	Downstream

Table 3.1: Fault classification based on monitor location.

It can be observed that the generated data is dominated by downstream faults based on the monitor location. The fault data generated is for all the above-mentioned fault locations and monitor locations. The fault data consists of all the possible faults (AG, BG, CG, AB, BC, AC, ABC, ABCG) with impedances 0.1, 0.5, 1.0, 1.5, and 2 ohms. The raw waveforms of voltages and currents have been extracted for the above-

mentioned cases at each power quality monitor. The overall simulation was 0.2 seconds, and the fault occurs between 0.06 and 0.14 seconds for a duration of 0.08 seconds. These voltage and current waveforms are sampled at a rate of 128 samples/cycle, corresponding to a sampling time of 130.2 μsec.

The fault data generated from the system was only restricted to a maximum fault impedance of 2 ohms because in most of the real-world scenarios, the faults are within the range of 0-2 ohms, and the faults with a fault impedance greater than 2 ohms can be categorized as high impedance faults [17]. These data samples are named according to the following convention:

M800F808_ABG_20_down

where,

M800 = Monitor at node 800

F808 = Fault at node 808

ABG = A phase to B phase to ground fault

20 = 2.0 ohms fault impedance on all the phases in the previous step

Down = Downstream fault with M800 and F 808

Consider the above-mentioned data sheet M800F808_ABG_20_down. The data is generated from EMTP, and the above three-phase waveforms are shown in Fig. 3.2.

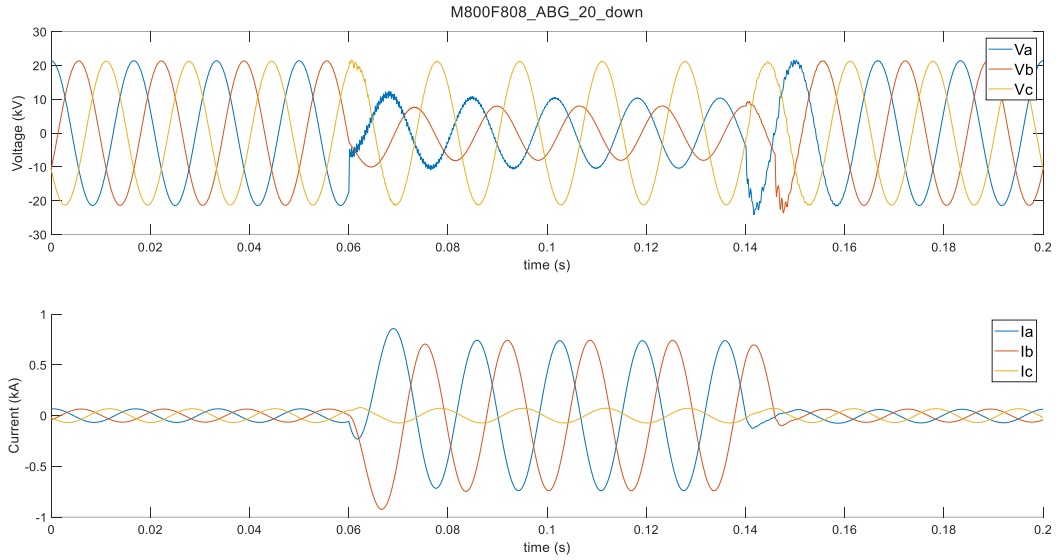

Figure 3.2: Three phase voltages and currents for M800F808_ABG_20_down event.

The data is generated using EMTP software and the output is through MPLOT in EMTP. MPLOT is a simulation waveform visualization function in EMTP [18]. The MPLOT function is entirely written using MATLAB and it is the compiled version of a set of m-files. The m-files contain MATLAB code, which can be either in the form of a script or a function. Using the MPLOT function available in EMTP mat-files can be generated. These mat-files consist of the MATLAB formatted data, and the data can be transformed accordingly. So, these mat-files are then converted into CSV files. Each CSV file consists of the time, instantaneous voltage, and current of three phases. As mentioned earlier, the time-step is 130.2083 μsec. A sample data sheet has been in Fig. 3.3.

	A	B	C	D	E	F	G
1	SourceName=IEEE_34_Bus_faults						
2	WhenStart=10/18/2022						
3	NominalBaseVoltage=14376.021						
4	NominalFundFreq=60						
5	SampleCount=1537						
6	Time(s)	Va	Vb	Vc	Ia	Ib	Ic
7	0	21410.34	-10650.5	-10627.7	66.05078	-41.7643	-18.9948
8	0.00013	21377.44	-9724.55	-11514	66.36842	-39.2894	-22.1573
9	0.00026	21291.4	-8773	-12371.2	66.54918	-36.737	-25.278
10	0.000391	21162.7	-7805.99	-13204.7	66.61793	-34.1254	-28.355
11	0.000521	20982.06	-6824.68	-14007.6	66.53061	-31.4289	-31.3616
12	0.000651	20757.32	-5831.34	-14778.5	66.28064	-28.6432	-34.2868
13	0.000781	20484.77	-4819.15	-15510.2	65.85799	-25.7754	-37.1261
14	0.000911	20159.4	-3789.39	-16202.1	65.2653	-22.8459	-39.8798
15	0.001042	19784.81	-2752.57	-16858.5	64.50918	-19.8665	-42.5399
16	0.001172	19364.87	-1712.49	-17475.8	63.58943	-16.8377	-45.0939
17	0.001302	18897.67	-669.454	-18050.1	62.50622	-13.761	-47.5349
18	0.001432	18379.83	374.8541	-18581	61.26928	-10.6422	-49.8581

Figure 3.3: Data format in the CSV files generated.

It can be observed in Fig. 3.3 that a base nominal voltage has been mentioned and this can be determined based on the monitor location. The first column represents the time step, and the next six columns represent the three-phase voltage and current data points. These data points can be plotted, and Fig. 3.2 can be obtained in the continuous time domain and Fig. 3.4 and Fig. 3.5 can be obtained in the discrete-time domain. For the monitor located at nodes 800 and 814, the nominal three-phase voltage is 24.9 kV; for single-phase, the nominal voltage is 14.376 kV as mentioned in Fig. 3.3. Similarly for the monitor located at node 888 the nominal three-phase voltage is 4.16 kV and for the single phase the nominal voltage is 2.401 kV.

The three-phase system of the IEEE 34-Bus system is slightly unbalanced initially due to the type of loads connected in the system. Moreover, this will ensure that there will always be a negative sequence component in the event of a balanced fault.

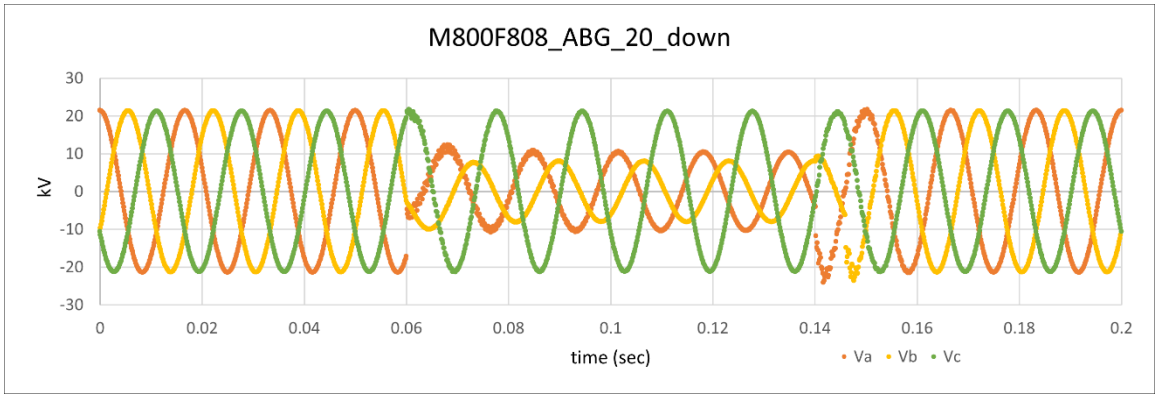

Figure 3.4: Discrete domain three-phase voltages for M800F808_ABG_20_down

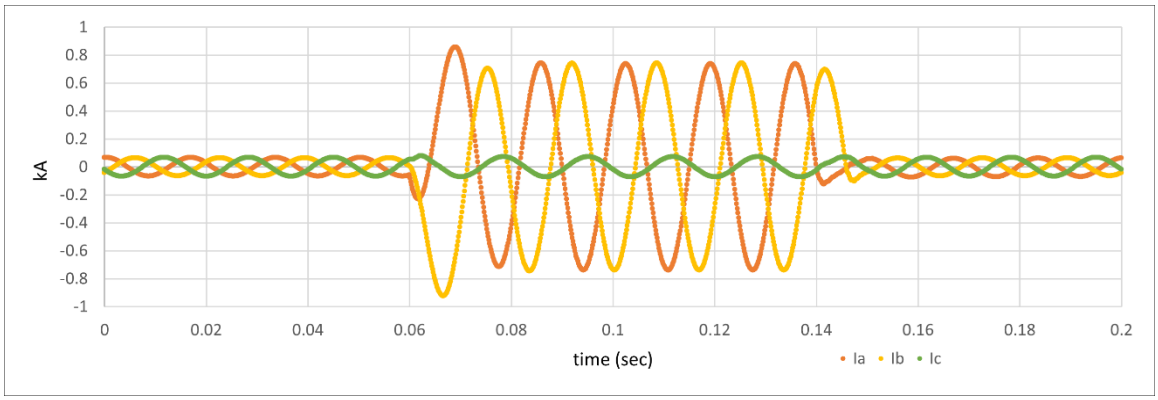

Figure 3.5: Discrete domain three-phase currents for M800F808_ABG_20_down

3.2 Sensitivity Analysis

Sensitivity analysis is an important part of mathematical modeling. In general, it can be defined as the study of the change in outputs when the inputs are altered [19]. In

most cases in power systems, sensitivity analysis is carried out to understand the stability of the power systems or for state estimation of the system. In this application, the sensitivity analysis can be defined as the change in the characteristics of the faults in the system based on the change in the characteristics of the transmission line/relay setting angle/maximum torque angle setting. This is an example of one-way sensitivity analysis in which a single variable is altered, and the effect of this variable is studied on the outcome.

In chapters 2.1 and 2.2, two techniques were discussed to estimate whether the fault is upstream or downstream. These both techniques can be implemented successfully by extracting the sequence components data from EMTP. But the characteristic angle in these both chapters can change the results of the fault direction beyond a certain limit. The sensitivity analysis tried to estimate the boundaries for the same by using the same fault data for different characteristics angle of the transmission line.

The main advantage of the sensitivity analysis is estimating the outcome (upstream/downstream) based on the data available from the angle which might include some errors. There are many advantages of sensitivity analysis if there are multiple inputs and a single output. In this case, the only input for the sensitivity analysis is the characteristic angle of the transmission line and the only output is the torque or impedance. This sensitivity analysis helps us to make informed decisions to set the maximum torque angle.

3.3 TORQUE SENSITIVITY ANALYSIS

In this section, the sensitivity analysis has been conducted for the torque calculated using (2.1). For convenience, the torque equation is re-written below:

$$T32Q = |V_2|\,|I_2|\,\cos\left(\angle - V_2 - (\angle I_2 + \angle MTA)\right)$$

It can be observed that the torque calculated can change polarity based on the cosine of the angle. The range of a cosine function is [-1,1] and the domain of the cosine function is [0, pi] or [0, 180] in degrees. For the example mentioned in Chapter 3.1, M800F808_ABG_20_down, the torque can be calculated as follows:

V_2 = 3918.762 V

I_2 = 195.947 A

$\angle V_2$ = -101.178 degrees → $\angle - V_2$ = 78.822 degrees

$\angle I_2$ = -4.046 degrees

Using the above equation and the MTA angle as 85 degrees (tentatively), the torque can be calculated as 767.3 kVA. The positive value of the torque indicates a downstream fault. The downstream fault is also known as a forward fault or fault in front of the relay location. Similarly, for an upstream fault M814_F808_ABG_20_up, the torque can be calculated as follows:

V_2 = 4979.358 V

I_2 = 13.59696 A

$\angle V_2$ = -117.443 degrees → $\angle - V_2$ = 62.557 degrees

$\angle I_2$ = -125.688 degrees

Using the above equation and the MTA angle as 85 degrees (tentatively), the torque can be calculated as -15.5 kVA. The negative value of the torque indicates an upstream fault. The upstream fault is also known as the reverse fault or fault at the back of the relay location. It can be observed that the change in magnitude of the torque is very high, and the values are not even close to zero.

For the sensitivity analysis, the MTA angle is the input variable and the torque calculated is the output variable. The sensitivity analysis for the above-mentioned equation has been done in this section.

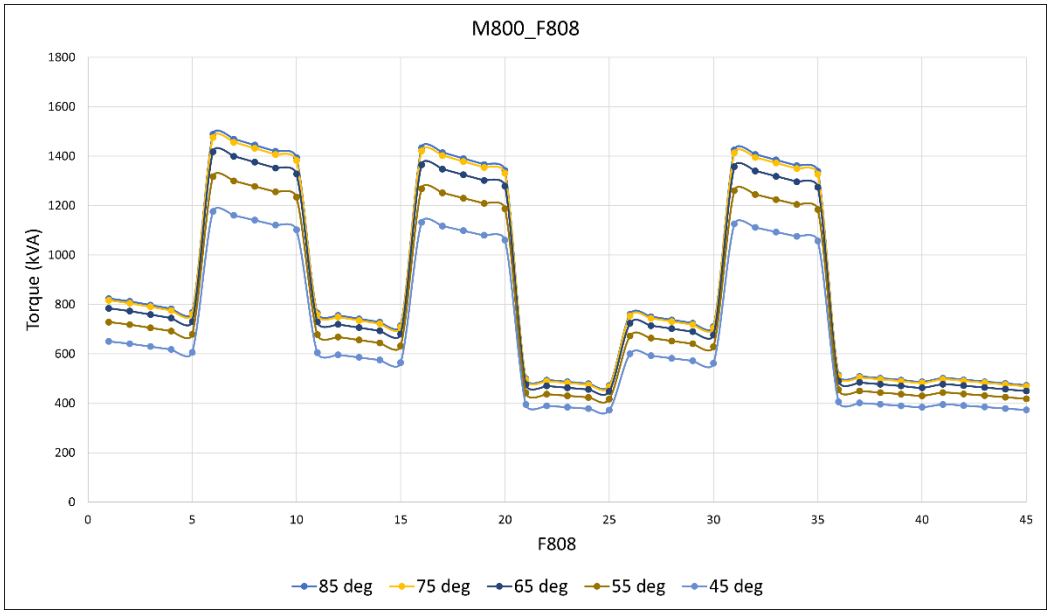

Figure 3.6: Torque Sensitivity Analysis for the M800_F808 case

Fig. 3.6 shows the sensitivity analysis scatter plot for the M800_F808 case. In this case, all the possible LG, LL, and LLG faults have been simulated with variable fault impedances of 0.1, 0.5, 1.0, 1.5, and 2.0 ohms. So, this corresponds to 5 (fault impedances) * 9 (fault types: AG, BG, CG, AB, BC, CA, ABG, BCG, ACG) to a total of 45 cases. In each case, the MTA angle in the torque has decreased by 10 degrees from 85 degrees. The torque has been calculated at monitor M800 for a fault at F808 which is a downstream fault. It can be observed that for all the values of the angles, the torque calculated is positive. This shows that the calculation of torque is insensitive and independent of the MTA angle if the angle is between 45 and 85 degrees. The reason for choosing the MTA angles between 45 and 85 degrees is because the MTA angle is also known as the negative sequence line impedance angle. This MTA angle can represent the angle of the line impedance angle in the negative sequence. The angle has been varied by 10 degrees for each step and the torque values for a downstream fault are plotted in Fig. 3.6.

Similarly, for the case, of M814_F808 (upstream) and M888_F808 (upstream) the torque plots have been plotted in Fig. 3.7 and Fig. 3.8. It can be observed that the torque values are negative which represents an upstream fault.

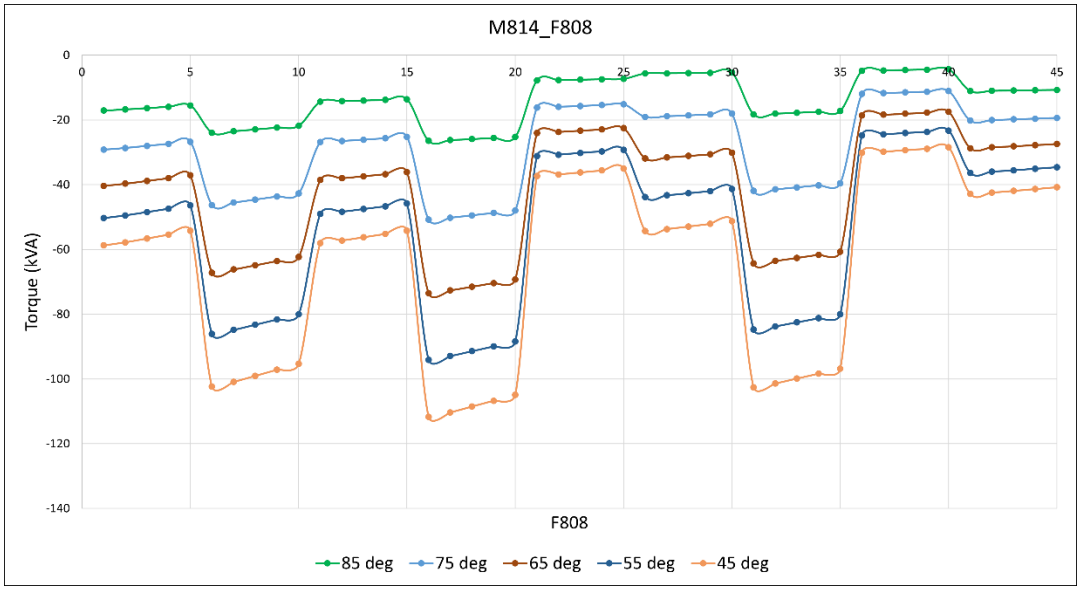

Figure 3.7: Torque Sensitivity Analysis for the M814_F808 case

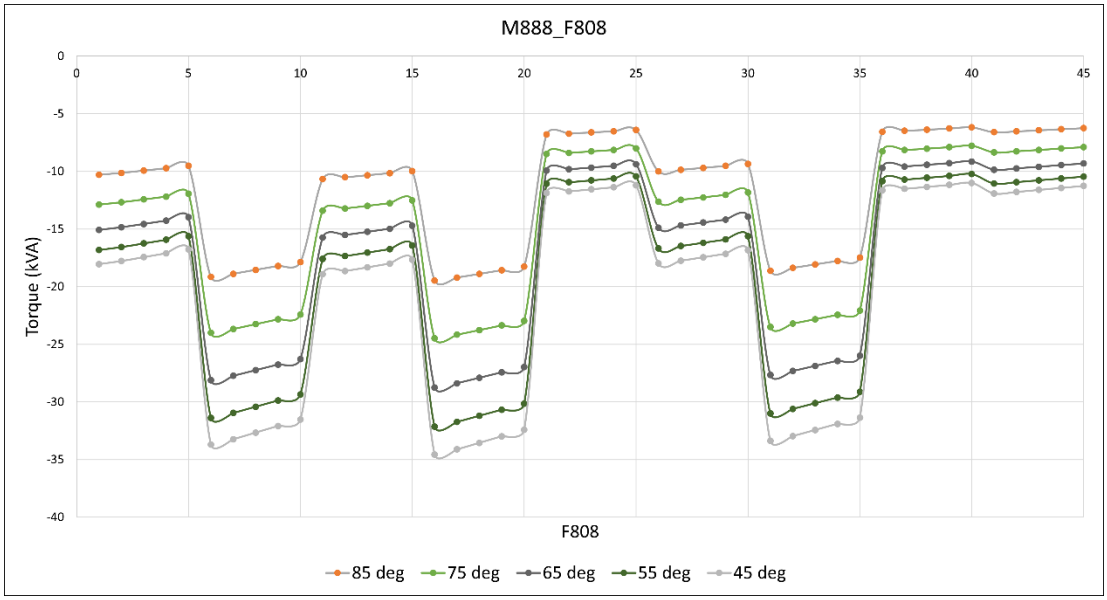

Figure 3.8: Torque Sensitivity Analysis for the M888_F808 case

Based on Fig. 3.6, Fig. 3.7, and Fig. 3.8, it can be observed that the calculation of torque is insensitive and independent- of the MTA angle if the angle is between 45 and 85 degrees. This is applicable both for the upstream and downstream faults in the system.

A similar kind of analysis has been done for the fault locations at nodes 824, 832, and 890. The results are very similar to the results shown in Fig. 3.6, Fig. 3.7, and Fig. 3.8 for the case fault at node 808.

3.4 Negative Sequence Impedance Sensitivity Analysis

In this section, the sensitivity analysis has been conducted for the negative sequence impedance measured for determining whether the fault is upstream or downstream using (2.3). For convenience, the impedance equation is rewritten below:

$$Z_{2measured} = \frac{\mathrm{Re}\,[V_2 * (1\angle Z_1 * I_2)^*]}{|I_2|^2}$$

It can be observed that the impedance measured can change the sign based on the positive sequence line angle. For example, as mentioned in chapter 3.1, M800F808_ABG_20_down, the impedance can be calculated as follows:

V_2 = 3918.762 V

I_2 = 195.947 A

$\angle V_2$ = -101.178 degrees

$\angle I_2$ = -4.046 degrees

Using the above equation and the positive sequence line angle as 85 degrees (tentatively), the impedance can be calculated as -19.985 ohms. The negative value indicated a downstream/forward fault location. Similarly, for an upstream fault M814_F808_ABG_20_up, the impedance can be calculated as follows:

V2 = 4979.358 V

I2 = 13.59696 A

$\angle V_2$ = -117.443 degrees

$\angle I_2$ = -125.688 degrees

Using the above equation and the positive sequence line angle at 85 degrees (tentatively), the impedance can be calculated as 83.9 ohms. The positive value of the impedance indicates a fault in the reverse/upstream/back of the relay location.

For the sensitivity analysis, the positive sequence line angle is the input variable and the torque calculated is the output variable. The sensitivity analysis for the above-mentioned equation has been done in this section.

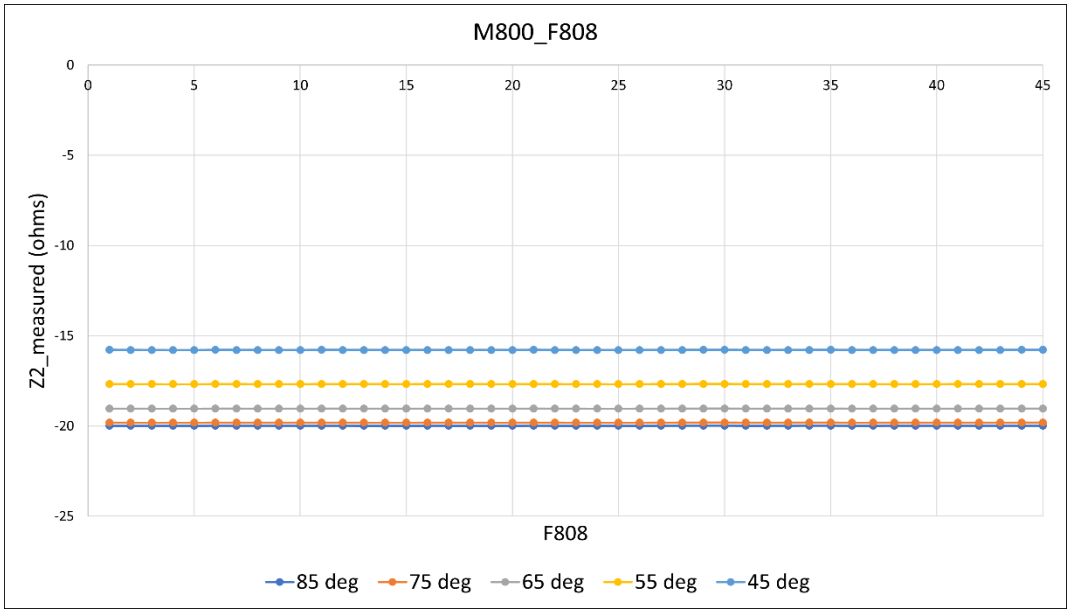

Figure 3.9: Negative sequence impedance Sensitivity Analysis for the M800_F808 case

Fig. 3.9 shows the negative sequence impedance sensitivity analysis plot for the M800_F808 case. In this case, all the possible types of LG, LL, and LLG faults have been simulated with variable fault impedances of 0.1, 0.5, 1.0, 1.5, and 2.0 ohms. So, this corresponds to 5 (fault impedances) * 9 (fault types: AG, BG, CG, AB, BC, CA, ABG, BCG, ACG) to a total of 45 cases. In each case, the negative sequence impedance angle in the torque has decreased by 10 degrees from 85 degrees and the impedance has been calculated at the monitor M800 for a fault at F808 which is a downstream fault. It can be observed that for all the values of the angles, the impedance calculated is negative. This proves that the calculation of impedance is independent of the angle if the angle is between 45 and 85 degrees. This angle can represent the angle of the line impedance angle in the negative sequence. The angle has been varied by 10 degrees for each step and the torque values for a downstream fault are plotted in Fig. 3.9.

Similarly, for the case, of M814_F808 (upstream) and M888_F808 (upstream) the impedance plots have been plotted in Fig. 3.10 and Fig. 3.11. It can be observed that the impedance values are positive which represents an upstream fault.

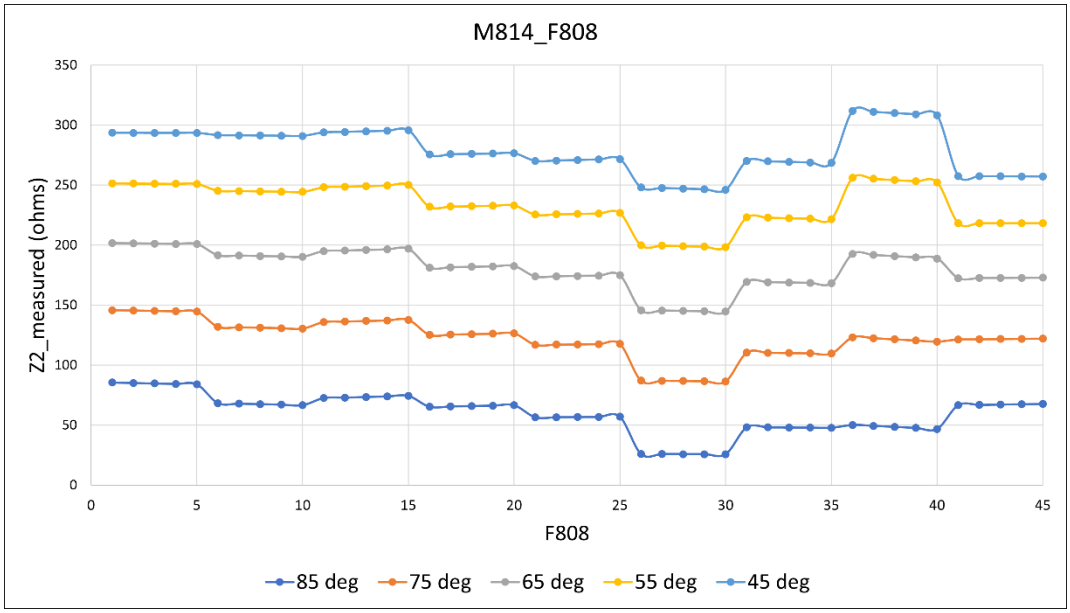

Figure 3.10: Negative sequence impedance Sensitivity Analysis for the M814_F808 case

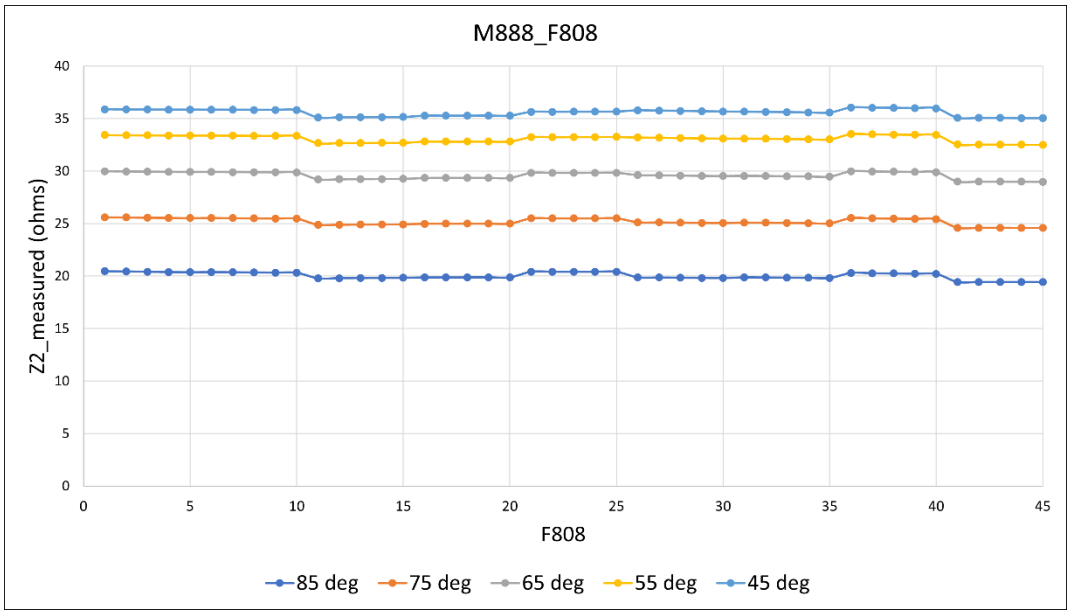

Figure 3.11: Negative sequence impedance Sensitivity Analysis for the M888_F808 case

Based on Fig. 3.9, Fig. 3.10, and Fig. 3.11, it can be observed that the calculation of impedance $Z2_{measured}$ is insensitive and independent- of the positive sequence line angle if the angle is between 45 and 85 degrees. This is applicable both for the upstream and downstream faults in the system.

A similar kind of analysis has been done for the fault locations at nodes 824, 832, and 890. The results are very similar to the results shown in Fig. 3.9, Fig. 3.10, and Fig. 3.11 for the case fault at node 808.

Chapter 4: Introduction to Neural Networks using TensorFlow.

In the previous chapter, the fault data was generated. This chapter introduces the basics of the neural network and TensorFlow basics. Before diving into TensorFlow [20], the basics of quantification and tensors are introduced.

The mathematical quantities commonly used in physics and engineering are scalar, vector, and tensor. A scalar quantity is a quantity that has only magnitude and no direction. A vector is a quantity that has both magnitude and direction. These are the most used components in engineering. Examples of scalars are hydrostatic pressure and temperature. Similarly, the examples of vectors are position, force, and velocity. A tensor is a quantity with multiple components and can be used to describe physical phenomena involving both magnitude and direction. They can be thought of as generalizations of vectors and matrices and have multiple dimensions. Examples of tensors are stress and strain. Scalars and vectors are also considered tensors of lower dimensions. Scalars are tensors of rank zero, vectors are rank one, and matrices as rank two. There are three types of tensors, and they can be classified as follows [21]:

1. Contravariant Tensors
2. Covariant Tensors
3. Mixed Tensors

In general, the contravariant vector can be defined as one that can be transformed as in the following:

$$A_i' = \sum_j \frac{\partial x_i'}{\partial x_j} A_j \tag{4.1}$$

Similarly, covariant vectors are a linear form and not a vector. The linear form is a mapping of vectors into scalars which is additive and homogeneous under multiplication by scalars [21]. The gradient is a prototype for a covariant vector which is defined as

$$\frac{\partial \varphi'}{\partial x_i'} = \sum_j \frac{\partial \varphi}{\partial x_j} \frac{\partial x_j}{\partial x_i'} \tag{4.2}$$

4.1 INTRODUCTION TO TENSORFLOW

Tensors are also an integral part of the data structure used by learning systems. The important properties of a tensor are shape and dType [22]. The shape of a tensor is determined by the number of dimensions along each axis. For example, a square matrix has dimensions (3,3) and a level 3 tensor can have (2,3,4) dimensions. The dType of the tensor refers to the type of data it contains. Some of the data types are float32, float64, unit8, int32, etc. The examples of the tensors in different dimensions are as follows [22]:

1. 0^{th} Dimension – Scalar
2. 1^{st} Dimension – Vector
3. 2^{nd} Dimension – Matrix
4. N^{th} Dimension – Tensor

The higher-order tensors are used to store time series data, JPEG images, and video data. Each dimension may correspond to the sample properties like height, size, width, color depth, frames, etc.... of the image/video. Machine learning techniques are being applied increasingly in all fields including power systems. TensorFlow is an open-source software library for dataflow and differentiable programming across a range of tasks [20]. It is a symbolic math library and is also used for machine learning applications such as neural networks. TensorFlow allows developers to create data flow graphics, which are structures that describe how data moves through a graph or a series of processing nodes. The nodes in the graph represent mathematical operations, while the edges represent the tensors that flow between them.

The main advantages of using TensorFlow are the flexibility and scalability offered. TensorFlow is designed to work with huge datasets and distributed systems, which makes it easier to scale up models for training and inference. For example, the neural network that will be implemented in the next chapter for the fault classification on the IEEE 34-Bus system can be expanded into a larger system with more buses. TensorFlow offers flexibility and control with features such as Keras Function API for the creation of complex topologies.

The main disadvantage of using TensorFlow is the steep learning curve and lack of transparency. The internal working of TensorFlow can be complex, which makes it difficult to understand the behavior of models. In the next chapter, the application of TensorFlow has been provided and it can be observed that the model can predict whether the fault is upstream or downstream in most cases, but the model fails to identify it in

certain cases. This might be attributed to the complexity of the model or several other factors which are discussed in Chapter 6.

4.2 Introduction to Types of Neural Networks and LSTM

This section explains the basic types of neural networks and the reasoning behind choosing LSTM for neural network training. There are mainly three types of neural networks namely:

1. Artificial Neural Network (ANN)
2. Convolution Neural Network (CNN)
3. Recurrent Neural Network (RNN)

ANNs are inspired by the functioning of the biological neural networks found in the brain. They consist of multiple hidden layers with multiple neurons. Each neuron receives an input signal which is processed by the activation function and the output is delivered to the next neuron with a specific weight. The learning methods in the ANN are classified into supervised learning, unsupervised learning, and reinforcement learning. In supervised learning the output is known and vice versa. In reinforcement learning the learning process is similar to supervised learning but the information available is less [23]. Tensors are also an integral part of the data structure used by learning systems. These are fully connected neural networks that can express very general functions [24].

CNNs can approximate a function invariant to location. The main applications of CNN are in image and video analysis. The working of CNN is based on the mathematical property of convolution. The input data is mostly an image which is handled by multiple

convolutional layers. Each layer applied a filter which is also known as a kernel to the input data, which is convoluted with the input image to extract the features.

RNNs can approximate functions related to time or related by sequence, such as dynamic systems [25]. One of the applications is the prediction of what's next. It can be a sequence or character, text, or event based on the inputs. The typical number of inputs is two which consists of the previous state of the system and the current input sequence. Complex dynamical systems are hard to model due to a lack of physics-based understanding. The main advantage of using RNN is the ability to handle input sequences of variable length. Some of the disadvantages are computational complexity and difficulty in capturing long-term dependencies. Since the topic under consideration is predicting whether the fault is an upstream or downstream event that is dependent on the previous system voltages and a time series of data, RNN will be implemented.

There are several variants of RNNs architectures. Some of them are as follows [25]:

1. Simple RNN Networks
2. Long Short-Term Memory (LSTM) Networks
3. Gated Recurrent Unit (GRU) Networks

LSTM Networks are designed to address the vanishing gradient problem which limits the ability to capture long-term dependencies in sequential data. They have complex update rules which allow the network to selectively remember or forget the information from previous time steps. By selectively updating and forgetting the information over a long duration, LSTM captures the long-term dependencies in

sequential data such as the waveforms of three-phase voltages and currents. As mentioned in Chapter 2, the sampling rate of the three-phase voltages and currents is 128 sample/cycle, and the simulation time is 0.2 sec. The number of time steps generated for a single event is 1537 values. The 1537 samples generated are for three-phase voltages and three-phase currents, including a time step. So, for a single event and a single monitor, the data produced is 1537*7 samples. But this is a single fault at a single monitor location. For a combination of 4 fault locations and 3 power quality monitor locations, the data set is 1537*7*4*3 data samples. But this data set is produced for all the fault types and 5 different fault impedances, which causes the final number of samples generated to be 1537*7*4*3*11*5. Since the data set used for training the neural network is very huge and it consists of sequential data, LSTM will be implemented. In the next chapter, neural network-based validation is discussed.

Chapter 5: Neural Network-Based Validation of Upstream and Downstream Faults

In the previous chapter, TensorFlow was introduced along with its advantages and disadvantages. In this chapter, neural network-based validation will be done to identify whether the fault is upstream or downstream. The development of the neural network model, training, and implementation of the neural network are discussed in this chapter. The comparison with the results in Chapter 3 is described in this chapter and the results and future work are discussed in the next chapter.

5.1 Training the Model Using Raw Voltage and Current Waveforms.

In this section, the data generation, training model, and parameters are explained. In Chapter 3, the data has been generated for various fault locations and fault types. But the initial data generated is sequential data for conducting sensitivity analysis, and the calculations of the torque and impedance. In modern power systems obtaining the sequential components data of the three-phase voltages and currents is difficult but obtaining the three-phase raw voltage and current phasors is easier from the recent developments in power quality measurement devices. The sampling rate initially was 128 samples/cycle, and this has been maintained constant. In this case, the same fault scenarios and monitor locations are considered but the data generated is the three-phase voltage and current waveforms. The data generated is in the same format as Fig. 3.3. The generated data of the raw waveforms (three-phase voltages and three-phase currents) are used for training the model. This is a step closer to identifying the faults using the raw waveforms instead of using the sequential components.

The major advantage of using the techniques mentioned in Chapter 3 is the simplicity of the techniques and implementation in a real-world scenario. Since the data is sequential, a bi-directional LSTM [26] will be implemented. The training of the neural network model is completed using Google colaboratory. The algorithm is as follows:

1. Defining a function to load all the data files. (The data generated is in the format of CSV as explained in Fig. 3.3)
2. Classifying the loaded data into up_samples and down_samples (for training and testing the data generated)
3. Normalizing the data using (5.1)
4. The data has been divided into a ratio of 7:3 for training and testing (this includes both upstream and downstream data)
5. Reshaping and shuffling the data for feeding the bi-directional LSTM model and the shape of the input variable is (1537,6) i.e., three-phase voltages and currents.
6. Defining the model with the activation function as sigmoid and 1 hidden layer.
7. Training the data and testing the data for accuracy

$$\hat{x} = \frac{x - \bar{x}}{\sigma_x} \tag{5.1}$$

where:

$\hat{x}$ = Normalized vector of the variable (voltage or current)

x = Actual data variable

$\bar{x}$ = Mean of the variable

σ_x = Standard deviation of the variable

The Python code uses various available packages like TensorFlow, Numpy, and Keras for ease of coding. The corresponding Python code for the same can be found in Appendix A. Since the activation function is the sigmoid function, the model calculates the probability of the data sample. The model creates a label 1 for the upstream faults and 0 for the downstream faults and calculates the probability of the fault event using the sigmoid function. The model then compares the probability with the labels. If the probability is greater than 0.5, the fault is classified as an upstream fault and vice versa.

5.2 Comparison with the Traditional Techniques (Three Monitors)

In the previous section, the neural network implementation was discussed. In this section, the neural network is trained using the data from the three monitors at nodes 800, 814, and 888. The results from the LSTM model have been discussed along with a comparison to the traditional techniques for the identification of the upstream or downstream fault. The LSTM model has been implemented and the accuracy of the test data is 100%. The accuracy is maximum and there might be several reasons for the same. The training data and the testing data are very similar to each other because the data generated is from the same fault event with varying impedances. Moreover, the data has been shuffled, but there are similarities between the waveforms. This can be observed in Fig. 5.1 and Fig. 5.2.

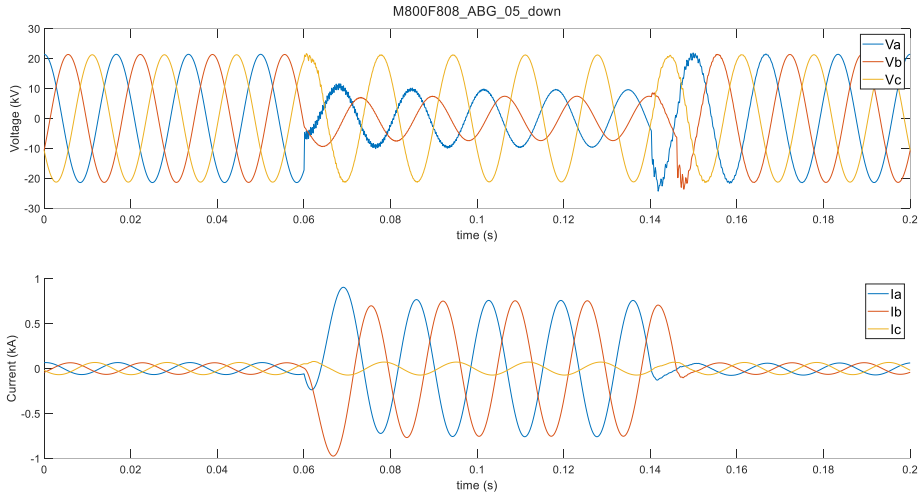

Figure 5.1: Three-phase voltages and currents for M800F808_ABG_05_down case.

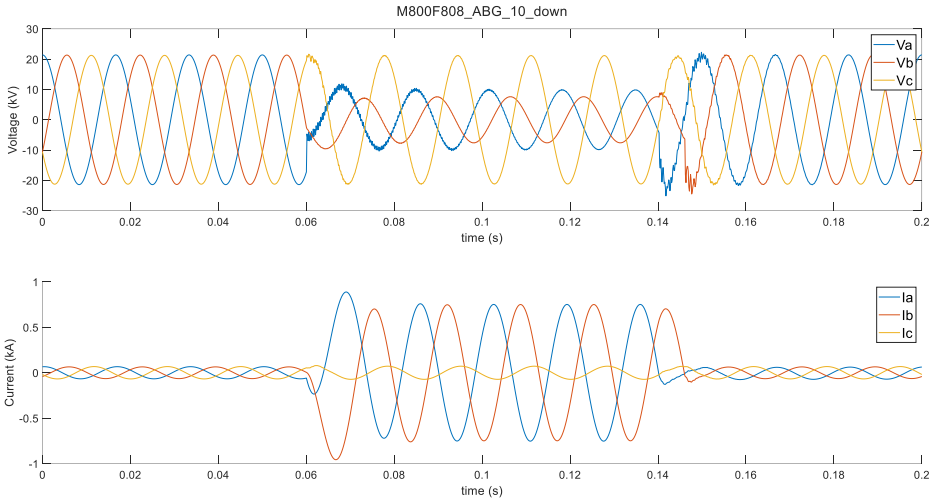

Figure 5.2: Three-phase voltages and currents for M800F808_ABG_10_down case.

It can be observed that the two waveforms are very similar, and the only difference is the magnitude of the voltage and current. The difference is so small that the model can easily identify the type of fault, and this leads to higher accuracy. Moreover, to

avoid the situation, the data has been shuffled and then trained to develop the model. The total generated data consists of the sample classification as mentioned in Table 5.1.

Sl. No	Training data	Testing data
Upstream Samples	154	66
Downstream Samples	308	132

Table 5.1: Classification of the samples for training and testing for three monitor's case

It can be observed that the training data is dominant with the downstream samples as mentioned in Table 5.1. To test the accuracy of the model, new data has been generated based on Fig. 5.3. The fault locations at nodes 808, 824, 832, and 890 are used for initial training and testing of the data. The new fault locations are at nodes 818, 840, 844, and 856. Since the transmission lines connecting to nodes 818 and 856 are single-phase, only single-phase fault data is produced and tested. Multiple data have been generated for varying fault durations and fault types with different fault impedances. The fault impedances vary from 0.1 to 3.7 ohms. A sample list of the fault data generated and tested has been provided in Table 5.2.

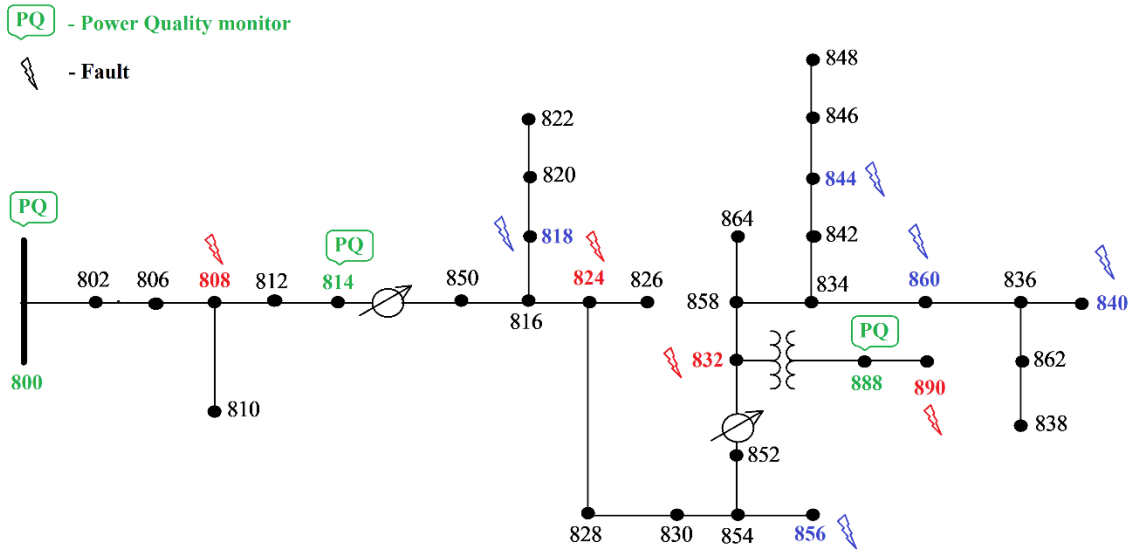

Figure 5.3: IEEE 34-Bus system with fault locations, PQ monitors, and new fault locations

Sl. No	Fault location	Monitor location	Fault Type	Classification based on		
				Torque	Negative sequence impedance	Neural Network
1	818	814	AG_10	Downstream	Downstream	Downstream
2	856	814	BG_01	Downstream	Downstream	Downstream
3	840	814	BG_37	Downstream	Downstream	Downstream
4	818	888	AG_01	Upstream	Upstream	Upstream
5	860	888	ACG_08	Upstream	Upstream	Upstream
6	840	888	AC_26	Upstream	Upstream	Downstream

Table 5.2: Comparison of fault identification using three different techniques.

It can be observed that in most cases, the trained LSTM model works perfectly but, in some cases, the model misclassifies an upstream fault as a downstream fault. There might be multiple reasons for the failure and some of them are insufficient training data which might be insufficient monitor locations, fault locations, different fault durations, and insufficient number of layers and epochs. Moreover, as mentioned earlier, the training data is dominated by downstream data samples. To resolve this issue, a new LSTM model has been implemented using the same parameters, but it has been trained with the data generated from a single monitor location. These details are mentioned in the next section.

5.3 Comparison with the Traditional Techniques (Single Monitor)

In the previous section, a neural network was trained to estimate whether the fault is upstream or downstream. The model can classify most of the events, but the accuracy is not 100% and one of the reasons might be the biased data. The data generated and trained is dominated by the downstream data and this might be one of the reasons for the failure of the model. To resolve this issue another neural network has been proposed but the data used for training the model is balanced (equal number of upstream faults and downstream faults). The monitor location is at node 814 and the fault data is generated at nodes 808 (upstream) and 824 (downstream) which includes all the types of faults (LG, LL, LLG, LLL, LLLG) with the fault resistances as 0.1, 0.5, 1.0, 1.5 and 2.0 ohms. The corresponding equivalent IEEE 34 bus system is shown in Fig. 5.4.

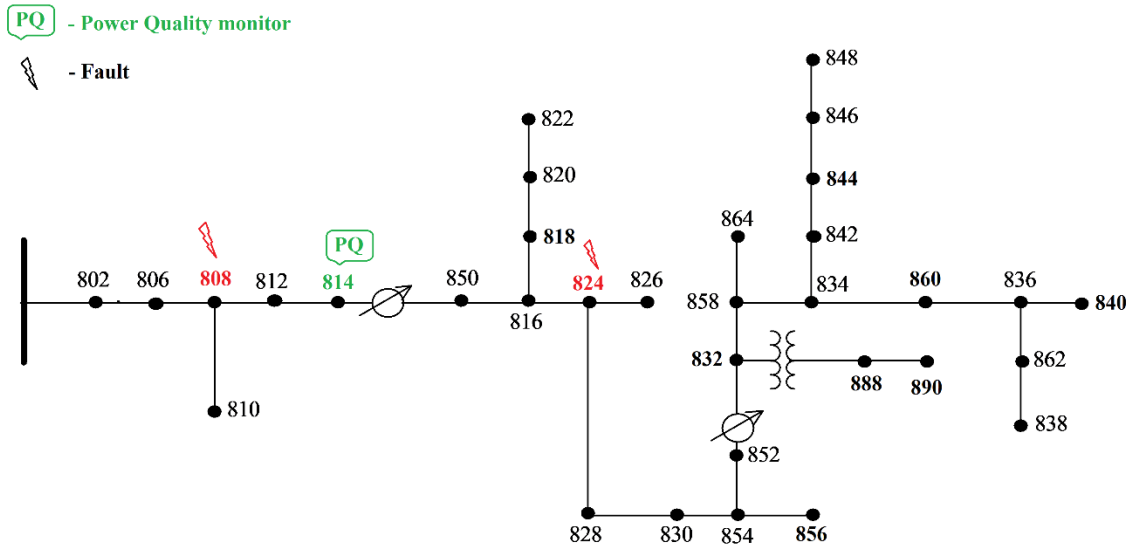

Figure 5.4: IEEE 34-Bus system for a single monitor location

The fault locations at nodes 808, 824, 832, and 890 are used for initial training and testing of the data. The new fault locations are nodes 818, 840, 844, and 856. Since the transmission lines connecting to nodes 818 and 856 are single-phase, only single-phase fault data is produced and tested. Multiple data have been generated for varying fault durations and fault types with different fault impedances. The fault impedances vary from 0.1 to 3.7 ohms. A sample list of the fault data generated and tested has been provided in Table 5.3.

Sl. No	Training data (Number of events)	Testing data (Number of events)
Upstream Samples	38	17
Downstream Samples	38	17

Table 5.3: Classification of the samples for training and testing for a single monitor.

The neural network has been trained as mentioned in section 5.1. The accuracy of the trained model is 94.74% but the test data which has been separated from the actual data has provided an accuracy of 100%. As mentioned earlier, the accuracy of the test data is high because of the similarities between the training data and testing data as shown in Fig. 5.1 and Fig. 5.2. The total generated data consists of the following sample classification as shown in Table 5.3. To test the actual performance of the model, new fault data has been generated. The new fault data consists of multiple fault types and fault impedances as some of them are at nodes 890, 856, 840, and 802. In most of these cases, the model has classified whether the fault is upstream or downstream. But in some of the cases for the faults at nodes 890, 840, and 818 the neural network fails and is unable to identify the downstream faults. For example, the M814F818_AG_10_down is a downstream fault from the monitor at node 814 and the neural network identifies it as an upstream fault. Similarly, for the case, M814F890_AB_15_down is a downstream fault, and the model identifies it as an upstream fault. These are some of the examples where the model is unable to identify the downstream faults.

Chapter 6: Conclusion and Future Work

This chapter presents the summary of the work done, the conclusion, and the scope for future work. The whole work done for the thesis can be sectioned into three parts, conducting a literature review and sensitivity of the techniques, generation of the fault data, and training the neural network using TensorFlow. In conducting the literature review, the references [14] and [15] are analyzed extensively and the robustness of the techniques is verified by conducting the sensitivity analysis. The literature review is also continued for three other references, but the techniques are not robust in comparison with [14] and [15]. The data generated consists of all types of faults with variable fault impedances ranging from 0.1 to 2.0 ohms. This data has been used for training neural networks. For the three monitors case, all the above-mentioned data has been used but for the single monitor data, the data corresponding to only a single monitor is used for training the model. The LSTM model has been trained using the data generated in TensorFlow and the accuracy is tested.

6.1 Conclusion

The thesis identifies the background and motivation to include machine learning techniques in power system protection. It can be observed that the techniques mentioned in sections 2.1 and 2.2 can classify the fault as an upstream fault or downstream fault with higher accuracy than the proposed neural network. But it can also be noted that the trained neural network can classify the faults in most of the cases but was unable to classify them in some of the cases. Since the model generates the probability of the fault being an upstream fault, the probability of the downstream faults in most of the cases is less than 0.25, but in the cases where the model was unable to identify the downstream

faults, the probability was around 0.51. If the probability calculated was less than 0.5, they would have been classified as a downstream fault. Since the applications of these techniques will be on the power system protection, even a small percentage of error can result in accurate estimation and might cause a system failure.

Thus, it can be summarized that neural networks have the potential to improve the accuracy and speed of fault detection and response in power systems. However, there are also challenges associated with the same. The challenge with the techniques is the lack of interpretability and explainability, huge data sets for training, and the challenge of ensuring the safety and reliability of the models. Further research development will be needed to address these challenges and fully realize the potential benefits of machine learning in power systems.

6.2 FUTURE WORK

There are several reasons why the trained neural network model was unable to classify the faults. Some of them are mentioned below along with the possible solutions for the same:

- Insufficient training data: The model has been trained with data from different power quality monitors with variable fault impedances. The data used for the training has the same fault timings and duration. They can be varied, and the performance of the model might be improved. Another reason might be insufficient monitor locations. A greater number of monitor locations can be included, and more data can be provided to train the model for higher accuracy.

The model was unable to classify some of the faults at node 840 and this might be from insufficient training data, as the fault at node 840 can be considered a remote fault. But for nodes 890 and 818, sufficient training data was available, but the model was unable to classify some of the faults. The model was unable to classify the fault at node 818. The reason might be the transmission line corresponding to the nodes connected to 818 is a single-phase line. The fault data corresponding to the single phase is not available for the model. This can be improvised by generating the fault data and using the same to train the model.

- Increase the size of the network: In the proposed model, only a single hidden layer has been proposed. Even with a single hidden layer in the neural network, the model was able to classify the direction of the faults in most cases. The performance of the model can be improved by introducing more hidden layers in the model. Increasing the number of hidden layers in the model makes the model complex but it can achieve the results with higher accuracy.
- Different activation functions: The activation function used for the training of the model is the sigmoid activation function. This function estimates the output between 0 and 1 which can also be assumed to be the probability of the output as 1. Instead of using the sigmoid, the tanh function can also be used to estimate the output. In this case, the output range is [-1,1]. The other functions that can be used are arctan, ReLU, etc....
- Parameters of the mode (batch size, optimizer, loss): In the LSTM model that has been implemented, the model has been trained with a batch size of 128, optimizer as Adam, and loss function as mean square error. For increasing the accuracy of the model, the batch size can be reduced to 64 or 32. The optimizer Adam can

also be replaced by other optimizers such as Gradient Descent, Stochastic Gradient Descent, Adagrad, etc....

- Physics-informed ML: Since the fault data generated and power flow follow the laws of physics, a recent new technique which is known as physics-informed neural networks can be used to improve the performance of the model. In these physics-informed neural networks, the model can embed the knowledge of any physical laws (such as power flow, ohm's law, etc....) that govern the data set in the learning process. This can increase the accuracy of the model.

The other scope of improvement in the model is modeling the high impedance faults. In the training of the model, the fault impedances are only varied between 0.1 to 2.0 ohms. But while testing the model, the impedances varied to 5.0 ohms and the model was able to classify many of the faults but not all of the cases. The model can be trained using the high impedance faults and the accuracy can be increased. In the model that has been developed, it has been trained to classify a single fault, and in the future, the model can be trained to classify multiple instantaneous faults in the system. Although the probability of occurrence of multiple instantaneous faults in the system is very low.

References

[1] Clare, "The relay market size is estimated to be USD 9.0 billion by 2022 and is projected to reach USD 14.7 billion by 2030, at a CAGR of 6.3%," GlobeNewswire, 03 March 2023. [Online]. Available: https://www.globenewswire.com/news-release/2023/03/03/2620171/0/en/The-relay-market-size-is-estimated-to-be-USD-9-0-billion-by-2022-and-is-projected-to-reach-USD-14-7-billion-by-2030-at-a-CAGR-of-6-3.html.

[2] P. Lim and D. Dorr, "Understanding and resolving voltage sag related problems for sensitive industrial customers," in *2000 IEEE Power Engineering Society Winter Meeting. Conference Proceedings*, Singapore, 2000.

[3] H. Hizman, P. Crossley, P. Gale and G. Bryson, "Fault section identification and location on a distribution feeder using travelling waves," in *IEEE Power Engineering Society Summer Meeting,*, Chicago, IL, USA, 2002.

[4] A. Girgis, C. Fallon and D. Lubkeman, "A fault location technique for rural distribution feeders," *IEEE Transactions on Industry Applications,* vol. 29, no. 6, pp. 1170 - 1175, 1993.

[5] M. Majidi, A. Arabali and M. Etezadi-Amoli, "Fault Location in Distribution Networks by Compressive Sensing," *IEEE Transactions on Power Delivery,* vol. 30, no. 4, pp. 1761 - 1769, 2014.

[6] J. Souza, M. Rodrigues, M. Schilling and M. D. C. Filho, "Fault location in electrical power systems using intelligent systems techniques," *IEEE Transactions on Power Delivery,* vol. 16, no. 1, pp. 59 - 67, 2001.

[7] D. Thukaram, H. Khincha and H. Vijaynarasimha, "Artificial neural network and support vector Machine approach for locating faults in radial distribution systems," *IEEE Transactions on Power Delivery,* vol. 20, no. 2, pp. 710 - 721, 2005.

[8] Q. Jin and R. Ju, "Fault Location for Distribution Network Based on Genetic Algorithm and Stage Treatment," in *2012 Spring Congress on Engineering and Technology*, Xi'an, China, 2012.

[9] L. Peretto, R. Sasdelli, E. Scala and R. Tinarelli, "Fault Location Method Integrating a Distributed Measurement System and Wavelet Analysis," in *2007 IEEE Instrumentation & Measurement Technology Conference IMTC 2007*, Warsaw, Poland, 2007.

[10] B. Fleming, "Schweitzer Engineering Laboratories," 24 - 26 February 1998. [Online]. Available: https://selinc.com/api/download/2475?id=2475.

[11] K. Zimmerman and D. Costello, "Fundamentals and improvements for directional relays," in *2010 63rd Annual Conference for Protective Relay Engineers*, College Station, TX, USA, 2010.

[12] *IEEE 34 Node Test Feeder,* 2010.

[13] E. S. T. Eldin, D. k. Ibrahim, E. M. Aboul-Zahab and S. M. Saleh, "High Impedance Faults Detection in EHV Transmission Lines Using the Wavelet Transforms," in *2007 IEEE Power Engineering Society General Meeting*, Tampa, FL, USA, 2007.

[14] J. Mahseredjian, "EMTP," 13 December 2017. [Online]. Available: https://www.emtp.com/documents/EMTP%20Documentation/doc/mplot/mplot.pdf.

[15] "Introduction to Tensors," TensorFlow, [Online]. Available: https://www.tensorflow.org/guide/tensor.

[16] A. Ng, "CS229: Machine Learning," 17 May 2022. [Online]. Available: https://cs229.stanford.edu/.

[17] I. Goodfellow, Y. Bengio and A. Courville, "Deep Learning, an MIT Press book," 2016. [Online]. Available: https://www.deeplearningbook.org/.

[18] S. F. Alwash, V. K. Ramachandaramurthy and N. Mithulananthan, "Fault-Location Scheme for Power Distribution System with Distributed Generation," *IEEE Transactions on Power Delivery*, vol. 30, no. 3, pp. 1187 - 1195, 2014.

[19] S. Gururajapathy, H. Mokhlis and H. Illias, "Fault location and detection techniques in power distribution systems with distributed generation: A review," *Renewable and Sustainable Energy Reviews*, vol. 74, pp. 949-958, 2017.

[20] K. Chen, J. Hu, Y. Zhang, Z. Yu and J. He, "Fault Location in Power Distribution Systems via Deep Graph Convolutional Networks," *IEEE Journal on Selected Areas in Communications*, vol. 38, no. 1, pp. 119 - 131, 2019.

[21] M. Mohammadi, R. Mundra and R. Socher, "CS224: Deep Learning for NLP," 2015. [Online]. Available: https://cs224d.stanford.edu/lecture_notes/LectureNotes4.pdf.

[22] F.-F. Li, R. Krishna and D. Xu, "Lecture 10: Recurrent Neural Networks," 29 April 2021. [Online]. Available: http://cs231n.stanford.edu/2021/slides/2021/lecture_10.pdf.

[23] M. Abadi, P. Barham, J. Chen, Z. Chen, A. Davis, J. Dean, M. Devin, S. Ghemawat, G. Irving, M. Isard, M. Kudlur, J. Levenberg, R. Monga, S. Moore, D. G. Murray, B. Steiner and P. Tucker, "TensorFlow: A System for Large-Scale Machine Learning," in *12th USENIX Symposium on Operating Systems Design and Implementation (OSDI '16)*, Savannah, GA, USA, 2016.

[24] M. Ginocchi, F. Ponci and A. Monti, "Sensitivity Analysis and Power Systems: Can We Bridge the," in *E.ON Energy Research Center, Institute for Automation of Complex Power Systems*, Aachen, Germany, 2021.

[25] P. Stefanidou-Voziki, N. Sapountzoglou, B. Raison and J. Dominguez-Garcia, "A review of fault location and classification methods in distribution grids," *Electric Power Systems Research*, vol. 209, no. 108031, 2022.

[26] W. Schlotter, "Tensors For Calculus," 20 May 2003. [Online]. Available: https://web.stanford.edu/~wschlott/one_page/tensors_old.pdf.